Effect of La doping on structural, optical and magnetic properties of BiFeO$_3$ thin films deposited by pulsed laser deposition technique

N. KUMAR, A. KAUSHAL, C. BHARDWAJ, D. KAUR[*]
Functional Nanomaterials Research Laboratory, Department of Physics and Centre of Nanotechnology,
Indian Institute of Technology Roorkee, Roorkee-247667, India

We report on the growth of Bi$_{1-x}$La$_x$FeO$_3$ (BLFO) thin films on quartz substrate using pulsed laser deposition (PLD) technique. The effect of varying La substitution on structural, optical and magnetic properties of BLFO thin films has been systematically investigated. X-ray diffraction (XRD) studies indicate rhombohedral structure of the (BLFO) films along highly oriented (011) peak. The crystallite size was found to increase with increase in La doping. The films show an average transmission of 80 % in the range of 200 – 2000 nm. The La doping in BiFeO$_3$ (BFO) affects the refractive index and optical bandgap. Magnetic studies reveal an enhancement in coercivity, remanent magnetization and susceptibility of the pure BFO films with La doping. The present study elucidates the effect of La doping on various properties of BFO films and that the optical behavior of BLFO films provide a reference for preliminary research to infrared detectors and optoelectronic devices.

1. Introduction

Multiferroic materials that simultaneously show electric and magnetic ordering are currently gaining more attention due to the fact that they are promising for the design of multifunctional devices and allow a direct integration of the material into the up-to-date semiconductor technology. Among various multiferroic materials, much attention has been paid to BiFeO$_3$ (BFO) in a thin film form, since it is one of those several compounds that exhibit multiferroicity at room temperature. It was reported to show *G*-type antiferromagnetic ordering with relatively high Neel temperature T$_N$ (370 °C) and ferroelectric ordering with high Curie temperature T$_C$ (830 °C) [1]. Powder X-ray diffraction (XRD) and neutron diffraction studies revealed that BiFeO$_3$ has a rhombohedrally distorted perovskite structure [2, 3]. The inhomogeneous magnetic spin structure of BiFeO$_3$ leads to the cancellation of macroscopic magnetization and inhibits the observation of the linear magnetoelectric effect. Previous studies suggest that the inhomogeneous magnetic spin structure can be effectively suppressed by La doping [4, 5]. Therefore, the influence of La doping on the magnetic properties of BiFeO$_3$ thin films deserves more attention.

In the present work, Bi$_{1-x}$La$_x$FeO$_3$ thin films were grown on quartz substrate by PLD technique due to its added advantage of being a non-equilibrium process. Moreover, PLD has been recognized as a promising versatile technique for the deposition of stoichiometric films of metal oxides at high deposition rate. Earlier we have reported the growth of Zn$_{1-x}$Mg$_x$O and Sr$_2$FeMoO$_6$ nanostructured double perovskite thin films by PLD technique [6, 7]. In the present study, we have tried to investigate the effect of La doping on various properties of BFO thin films deposited on quartz substrate by PLD technique. The grain size, remanent magnetization, coercivity and susceptibility have been shown to be influenced by La doping in BFO thin films. Also, the optical properties of La doped BiFeO$_3$ films are investigated and thus a reference is provided for preliminary research into infrared detectors and optoelectronic devices. A control of the optical bandgap between 2.68 to 2.60 eV has been obtained with La doping content in BFO films on quartz substrate in spite of the large lattice mismatch between substrate and BFO films.

2. Experimental

Thin films of Bi$_{1-x}$La$_x$FeO$_3$ (BLFO) with $x = 0$, 0.02, 0.05, 0.1, 0.2 and 0.3 were grown on quartz substrates by pulsed laser deposition technique using a 15 mm diameter target. The details of process setup are given elsewhere [6]. The targets were prepared by mixing appropriate molar ratios of Bi$_2$O$_3$, Fe$_2$O$_3$ and La$_2$O$_3$ powders. After 8 hours of grinding, the mixed powder was calcined in air at 600 °C for 2 hours. The powder was further reground and pressed into pellets by applying pressure of 80 MPa. Finally, it was sintered at 870 °C for 5 minutes by rapid thermal process. The KrF excimer laser (248 nm, 10 Hz) with energy of 300 mJ was used for the deposition. The substrate temperature was maintained at 600 °C with oxygen pressure of 50 mTorr and deposition time of 35 minutes. Before ablation, the chamber was evacuated to a base pressure of 10^{-6} Torr, and then the pure oxygen was introduced through a mass flow controller. The chamber pressure was measured using a combination vacuum gauge (Pfeiffer Vacuum) and maintained at a pressure of 50

mTorr. Before every deposition, the target was pre-ablated for 1 minute in order to ascertain the same state of the target in every deposition. After the deposition, the films were annealed at 700 °C for 30 minutes for crystallization. The films are allowed to cool in the chamber naturally.

The orientation and crystallinity of the films were studied using Bruker D8 Advanced Diffractometer of Cu Kα (1.54Å) radiations in (θ-2θ) geometry. The surface morphology of the films were analyzed using atomic force microscopy in semi contact mode (AFM, NTMDT) with silicon nitride (Si$_3$N$_4$) tip of 10 nm radius. Optical properties in the wavelength range of 200-2000 nm were studied using a UV–VIS-NIR spectrometer. The magnetic properties of the films were measured using superconducting quantum interference device (Quantum Design).

3. Results and discussion

3.1 Structural properties

Fig. 1 shows the XRD pattern for Bi$_{1-x}$La$_x$FeO$_3$ (x = 0, 0.02, 0.05, 0.1, 0.2, 0.3) thin films deposited on quartz substrates. All peaks of the films are indexed to a rhombohedral structure with preferred orientation along (110) direction. A few low intensity additional peaks at 2θ= 28.32 and 29.12 were found in case of pure BFO thin films (x = 0) which could be due to formation of Bi$_2$Fe$_4$O$_9$ oxide phases. La doping to BFO results in elimination of these additional impurity phases with increase in intensity of the (110) peaks. The crystallite size calculated from XRD pattern was found to increase from 24.62 nm to 53.14 nm with corresponding increase in La doping from x = 0 to x = 0.3 and the values are described in Table 1. The increase in grain size could be due to the bigger ionic radii of La^{3+} (103.2 pm) than that of Bi^{3+} (103 pm) ion which get replaced on La doping. From XRD patterns, it is clear that La doping provides phase purity and stabilizes the perovskite structure. Repeated measurements suggest that the elimination of secondary phases is not due to mixing related effect but due to the effect of La doping. This observation can be qualitatively substantiated with the thermodynamics along with Pauling's equation [8] which relates ionic bond strength (I$_{AB}$) with the average electronegativity of cation (χ_A) and anion (χ_B) as shown in following equation:

$$I_{AB} = 1 - \exp[-(\chi_A - \chi_B)/4] \qquad (1)$$

Table 1. Calculated crystallite size, refractive index and optical band gap of Bi$_{1-x}$La$_x$FeO$_3$ thin films with different La content (x).

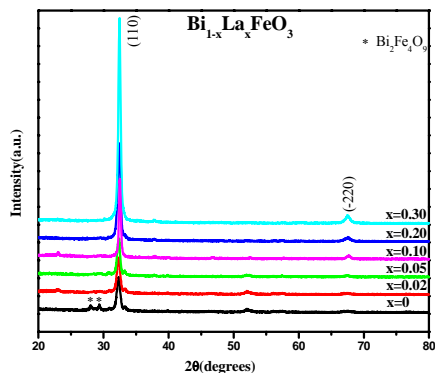| La Content (x)	Crystallite size (nm)	Refractive index (at 700 nm)	Optical bandgap (eV)
0	24.62	2.10	2.68
0.02	29.80	2.14	2.71
0.05	30.80	2.22	2.70
0.1	31.76	2.30	2.66
0.2	41.52	2.47	2.61
0.3	53.14	2.53	2.60

Fig. 1. XRD pattern of deposited Bi$_{1-x}$La$_x$FeO$_3$ thin films.

Table 2 shows the electronegativity values of various A-site cations (Bi^{3+} and La^{3+}) and anion (O^{2-}). The values of ionic bond strength were calculated using above equation (1). The ionic bond strength of La–O bond is found to be higher than the Bi–O bond. This may lead to reduced enthalpy of formation (ΔH$_f$) of La-doped BiFeO$_3$ as compared to undoped BiFeO$_3$ as ΔH$_f$ is a function of bond strength as follows:

$$\Delta H_f = P_{AB} (\varepsilon_{AB} - 1/2(\varepsilon_{AA} + \varepsilon_{BB}) \qquad (2)$$

where P$_{AB}$ is the number of A–B bonds and ε represents that bond energy which becomes increasingly more negative as the bond strength increases. This can reduce the free energy of formation (ΔG$_f$) of La-doped BiFeO$_3$

phase as compared to undoped $BiFeO_3$ phase. ΔG_f may become more negative if entropy change is positive considering La–O bond replaces Bi–O bond in the lattice randomly. This will make La-doped $BiFeO_3$ phase more stable than pure $BiFeO_3$. The 2D AFM images of the BLFO thin films with scan area of 1 μm × 1 μm are illustrated in Fig. 2. The uniformity in the surface was found to decrease with increase in La content. Also, the grain size increases with increase in La composition, which is in accordance with the XRD results.

Table 2. Ionic bond strength of Bi-O and La-O bond.

Species	Electronegativity	Ionic strength of bond with O^{2-} (electronegativity = 3.44)
Bi^{3+}	2.02	0.30
La^{3+}	1.1	0.44

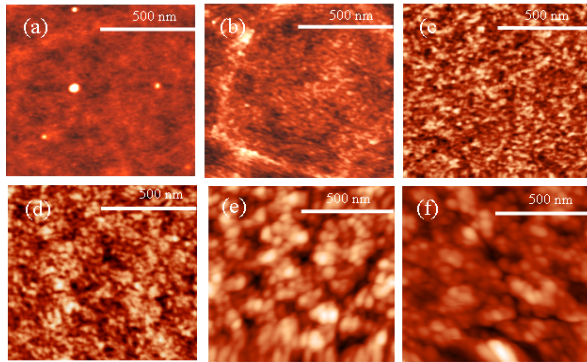*Fig. 2. AFM micrographs of $Bi_{1-x}La_xFeO_3$ thin films for (a) x = 0, (b) x = 0.02, (c) x = 0.05, (d) x = 0.1, (e) x = 0.2 and (f) x = 0.3.*

3.2 Optical properties

Fig. 3 shows the optical transmission spectra of BLFO thin films with La content $x = 0$ to $x = 0.3$ in the wavelength ranging from 200 nm to 2000 nm. All the films are highly transparent with an average transmittance of about 80%. There was a gradual shift of transmission edge towards a longer wavelength with corresponding increase in La doping as shown in inset in Fig. 3. The refractive index (n) was estimated from the transmission spectrum by using the Swanepoel's envelope method [9], and the following expression was used to calculate the refractive index:

$$n = \left[N + \left(N^2 - n_0{}^2 n_1{}^2 \right)^{1/2} \right]^{1/2} \qquad (3)$$

Where

$$N = \frac{n_0{}^2 + n_1{}^2}{2} + 2n_0 n_1 \frac{T_{max} - T_{min}}{T_{max} T_{min}} \qquad (4)$$

and n_0 and n_1 (1.46 in our case) are the refractive index of air and substrate, respectively. T_{max} and T_{min} are maximum and minimum transmittance values at the same wavelength. Fig. 4 represents the refractive indices (n) variation with wavelength (λ) for the films of different La composition. Refractive index of the films decreases with increase in wavelength, which shows the normal dispersion behavior. Also, the values of refractive indices (n) evaluated at a fixed wavelengths of 700 nm were found to increase with corresponding increase in La doping in BLFO films as shown in Table 1. This could be due to the change in stoichiometry and internal strain caused with the addition of La in $BiFeO_3$.
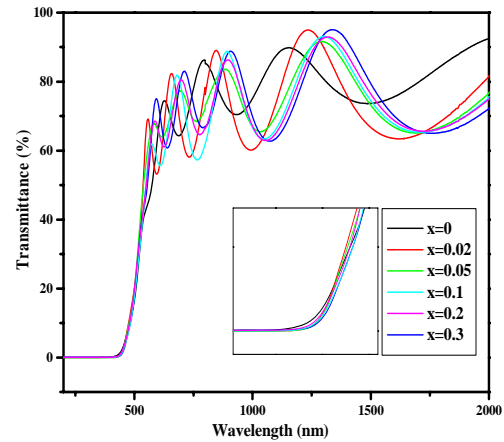

Fig. 3. Transmittance spectra of $Bi_{1-x}La_xFeO_3$ thin films of different La contents (x).
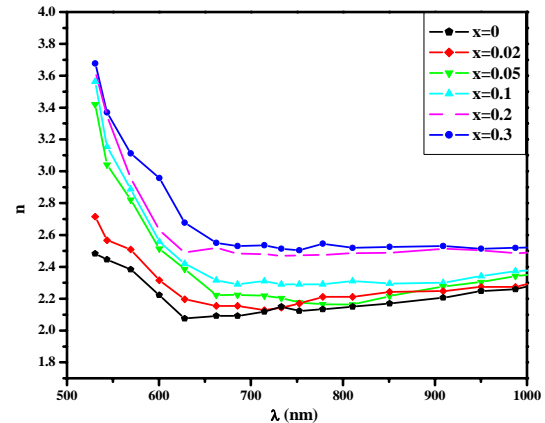

Fig. 4. Refractive index (n) variations with wavelength (λ) of $Bi_{1-x}La_xFeO_3$ thin films.

The optical absorption coefficient α is calculated from the following relation [10]:

$$T = \frac{(1-R)^2 \exp(-\alpha t)}{1 - R^2 \exp(-2\alpha t)} \quad (5)$$

where R and T are the spectral reflectance and transmittance and t is the film thickness. For greater optical density $(\alpha t > 1)$, the interference effects due to internal reflections as well as reflectance at normal incidence are negligible, and the previous equation can be approximated as:

$$T \approx \exp(-\alpha t) \quad (6)$$

The optical absorption coefficient α is given by the approximate formula,

$$\alpha = -\frac{1}{t} \ln T \quad (7)$$

where t is the film thickness and T the transmittance measured. The direct and indirect band gap of the films was calculated using the Tauc relationship as follows [11]:

$$\alpha h\upsilon = A(h\upsilon - E_g)^n \quad (8)$$

where α is the absorption coefficient, A is a constant, h is the Planck's constant, υ is the photon frequency, E_g is the energy band gap and n is ½ for direct band gap semiconductor. An extrapolation of the linear region of a plot of $(\alpha h\upsilon)^{\frac{1}{n}}$ on the y-axis versus photon energy $(h\upsilon)$ on the x-axis gave the value of the energy band gap E_g.

Since $E_g = h\upsilon$ when $(\alpha h\upsilon)^{\frac{1}{n}} = 0$, here the direct band gap of the BLFO thin films was evaluated by extrapolating the straight line part of the curves $(\alpha h\upsilon)^2 = 0$ as shown in Fig. 5. At small La doping $x = 0.02$, the value of band gap is more than that of undoped sample (Fig. 6). This may be due to the presence of $Bi_2Fe_4O_9$ impurities in the undoped sample leading to a smaller band gap. With further increase in La doping, the band gap decreases and the value of 2.61 eV was observed at maximum La doping i.e. at $x = 0.3$ (Table 1). The decrease in band gap (red shift) is due to the La doping in $BiFeO_3$ that brings about a compositional change of the host network. In the fundamental absorption region, the absorption is due to the transition from the top of valence band to the bottom of the conduction band. Addition of La in $BiFeO_3$ thin film may cause an increase in the density of state in the valence band. The addition of La may also create localized states in the band gap. This will lead to a shift in the absorption edge towards lower photon energy, and, thus a decrease in the optical energy gap.
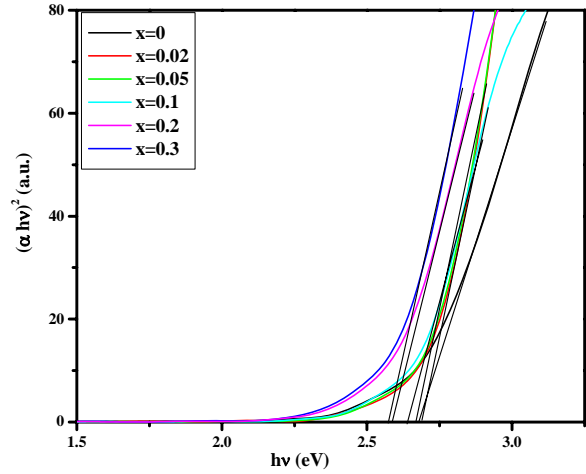

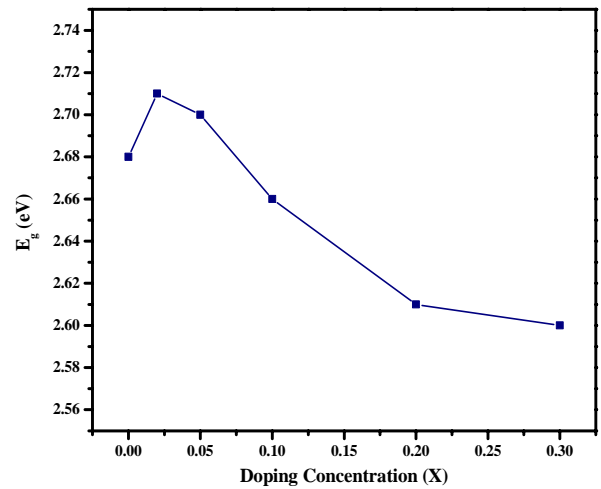Fig. 5. $(\alpha h\upsilon)^2$ vs. $h\upsilon$ plot of $Bi_{1-x}La_xFeO_3$ thin films of different La contents.

Fig. 6. Variation of band gap of $Bi_{1-x}La_xFeO_3$ thin films with different La contents.

3.3 Magnetic properties

Fig. 7 (a & b) shows the magnetization M versus applied field H of $BiFeO_3$ and $Bi_{0.9}La_{0.1}FeO_3$ thin films at 300K and 5K respectively. At 300 K (Fig. 7a), the magnetization for undoped $BiFeO_3$ was found to be very small which varies almost linearly with the field as expected for an antiferromagnetic material. There was no sign of saturation found in it. The small magnetization could be due to spin-canting in the antiferromagnetic $BiFeO_3$. With addition of La in $BiFeO_3$, the magnetization increases and tends to saturate at 6.8 emu/cm³ alongwith an increase in coercivity for La content x=0.1. There is enhancement in remanent magnetization from 0.26 emu/cm³ to 1.86 emu/cm³. At 5 K (Fig. 7b), the addition of La to $x = 0.1$ in $BiFeO_3$ causes the remanent magnetization to increase from 2.46 emu/cm³ to

2.6 emu/cm³. Table 3 gives the saturation magnetization (M_S), remanent magnetization (M_R) and coercivity (H_C) value for undoped and La doped BiFeO₃ thin films at temperatures 300 K and 5 K respectively.
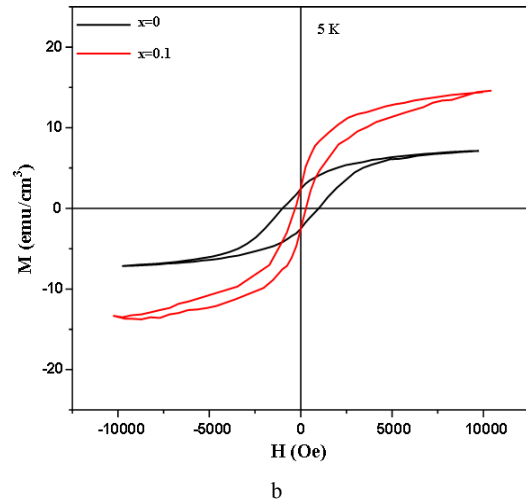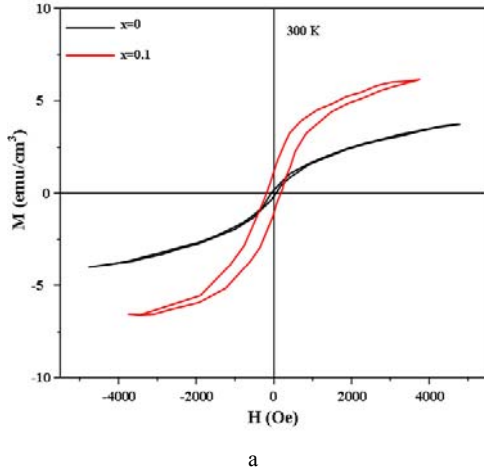

a

b

Fig. 7. M-H curve for $Bi_{1-x}La_xFeO_3$ thin films with $x = 0$ and $x = 0.1$ at (a) 300K and (b) 5K temperatures.

Table 3. Comparison of M_S, M_R and H_C of $Bi_{1-x}La_xFeO_3$ thin films.

La content (x)	Temperature (K)	M_S (emu/cm³)	M_R (emu/cm³)	H_C (Oe)
0	300	---	0.26	94
0.1	300	6.8	1.86	202
0	5	7.5	2.46	920
0.1	5	14.8	2.6	523

Fig. 8 shows the temperature variation of magnetization and susceptibility of BiFeO₃ and Bi₀.₉La₀.₁FeO₃ thin films at an applied field (H) of 1000 Oe. We observe that the La doping enhances the magnetization of the film and hence enhances the susceptibility. In this ZFC curve we observe a sharp cusp around 50 K, which is near to the observed blocking temperature T_B in antiferromagnetic material γ-Fe₂O₃ (at 72 K) [12]. This temperature is defined as a typical blocking process of an assembly of superparamagnetic spins [13]. The enhancement of magnetic parameters with La addition could be due to increased magnetoelectric coupling [14]. The antiferromagnetic ordering in the multiferroic BiFeO₃ is perpendicular to the ferroelectric polarization. The applied magnetic field causes the electric polarization in the sample due to magnetoelectric effect [15]. The ferroelectric polarization corresponds to a fictitious magnetic field along the direction of polarization; the sublattice spin will rotate symmetrically towards its direction under this effect. So the system takes on ferromagnetic ordering in the direction of ferroelectric ordering due to this magnetoelectric coupling. On addition

of La in BiFeO₃, the ferroelectric polarization increases which causes the magnetoelectric effect to increase and thus the ferromagnetic ordering increases in the antiferromagnetic BiFeO₃ leading to an increase in magnetism.
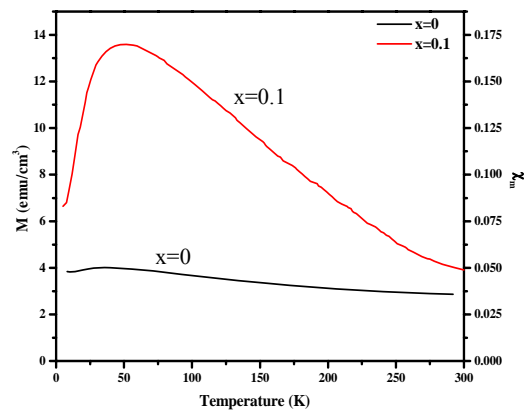

Fig. 8. M-T and χ_M –T curve for $Bi_{1-x}La_xFeO_3$ thin films with $x = 0$ and $x = 0.1$ at applied field H = 1000 Oe.

4. Conclusion

$Bi_{1-x}La_xFeO_3$ thin films with x = 0, 0.02, 0.05, 0.1, 0.2, 0.3 were grown on quartz substrate using pulsed laser deposition technique. All the films were found to exhibit rhombohedral structure with preferred (110) orientation. The La substitution at Bi site eliminated the small impurity phases of undoped $BiFeO_3$ and stabilized the crystal structure. The crystallite size calculated from XRD pattern was found to increase with increase in La doping. The refractive index at 700 nm wavelength was found to increase from 2.10 to 2.53 with corresponding increase in La content from x = 0 to x = 0.3. The optical band gap of $BiFeO_3$ thin films was found to decrease from 2.68 eV to 2.60 eV with corresponding increase in La doping from x = 0 to x = 0.3. The optical properties render it as a suitable candidate for the IR detectors and optoelectronic devices. Also, ferromagnetic properties at 5 K and 300 K are enhanced by La doping in $BiFeO_3$ thin films. The remanent magnetization at room temperature increases from 0.26 emu/cm^3 for x = 0 to 1.86 emu/cm^3 for x = 0.1.

References

[1] F. Gao, C. Cai, Y. Wang, S. Dong, X. Qiu, G. Yuan, Z. Liu, J. Appl. Phys. **99**, 094105 (2006).
[2] J. M. Moreau, C. Michel, R. Gerson, W. J. James, J. Phys. Chem. Solids **32**, 1315 (1971).
[3] Y. H. Chu, L.W. Martin, M. B. Holcomb, R. Ramesh, Mater. Today **10**, 16 (2007).
[4] S. R. Das, P. Bhattacharya, R. N. Choudhary, R. S. Katiyar, J. Appl. Phys. **99**, 066107 (2006).
[5] A. Z. Simoes, L. S. Cavalcante, C. S. Riccardi, J. A. Varela, E. Longo, Current Appl. Phys. **9**, 520 (2009).
[6] A. Kaushal, D. Kaur, Solar Energy Material and Solar Cells, **93**, 193 (2009).
[7] D. Kumar, D. Kaur, Physica B, **405**, 3259 (2010).
[8] K. Singh, S. A. Acharya, S. S. Bhoga, Ionics **12**, 295 (2006).
[9] R. Swanepoel, J. Phys. E: Sci. Instrum. **16**, 1214 (1983).
[10] Z. S. El-Mandouh, M. S. Selim, Thin Solid Films **371**, 259 (2002).
[11] Y. Xu, M. Shen, Mater. Lett. **62**, 3600 (2008).
[12] B. Martinez, X. Obradors, L. Balcells, A. Rouanet, C. Monty, Phys. Rev. Lett. **80**, 181 (1998).
[13] T. J. Park, G. C. Papaefthymiou, A. J. Viescas, A. R. Moodenbaugh, S. S. Wong, Nano Lett. **7**, 766 (2007).
[14] N. Wang, J. Cheng, A. Pyatakov, A. K. Zvezdin, J. F. Li, L. E. Cross, D. Viehland, Phys. Rev. B **72**, 104434 (2005).
[15] M. Fiebig, J. Phys. D: Appl. Phys. **38**, R123, (2005).

_____
*Corresponding author: dkaurfph@iitr.ernet.in